Interactions of human serum albumin with phosphate and Tris buffers: impact on paclitaxel binding and nanoparticles self-assembly

A. H. Gonzalez-Posada, M. Mesa, L. Sierra & B. Lopez

Published online: 13 Sep 2024.

Submit your article to this journal ↗

Article views: 68

View related articles ↗

View Crossmark data ↗

Taylor & Francis
Taylor & Francis Group

RESEARCH ARTICLE

🔓 OPEN ACCESS   Check for updates

Interactions of human serum albumin with phosphate and Tris buffers: impact on paclitaxel binding and nanoparticles self-assembly

A. H. Gonzalez-Posada, M. Mesa, L. Sierra and B. Lopez

Materials Science Group, Institute of Chemistry, University of Antioquia, Medellín, Colombia

ABSTRACT

Aim: To investigate the conformational changes in human serum albumin (HSA) caused by chemical (CD) and thermal denaturation (TD) at pH 7.4 and 9.9, crucial for designing controlled drug delivery systems with paclitaxel (PTX).

Methods: Experimental and computational methods, including differential scanning calorimetry (DSC), UV-Vis and intrinsic fluorescence spectroscopy, mean diameter, polydispersity index (PDI), ζ-potential, encapsulation efficiency (EE), *in vitro* release and protein docking studies were conducted to study the HSA denaturation and nanoparticles (NPs) preparation.

Results: TD at pH 7.4 produced smaller NPs ($287.1 \pm 12.9\,nm$) than CD at pH 7.4 with NPs ($584.2 \pm 47.7\,nm$). TD at pH 9.9 exhibited high EE ($97.3 \pm 0.2\%$w/w) with rapid PTX release (50% within 1h), whereas at pH 7.4 ($96.4 \pm 2.1\%$w/w), release only 40%. ζ-potentials were around $-30\,mV$.

Conclusion: Buffer type and pH significantly influence NP properties. TD in PBS at pH 7.4, provided optimal conditions for a stable and efficient drug delivery system.
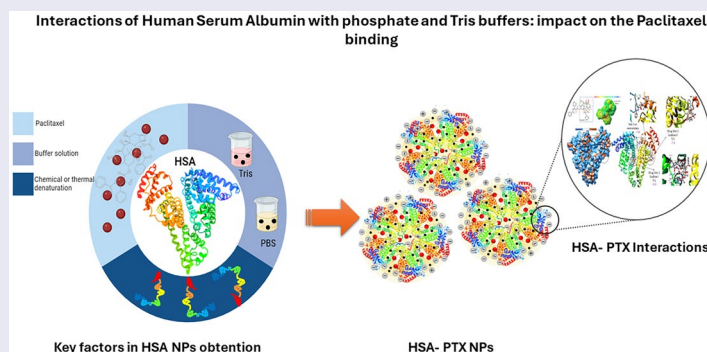
GRAPHICAL ABSTRACT

1. Introduction

Paclitaxel (PTX) is one of the most effective antitumor chemotherapeutic treatments developed, displaying a wide spectrum of activity. However, due to its limited solubility, the use of formulations causes adverse negative effects. Therefore, implementing alternative strategies to enhance PTX solubility becomes necessary (Ma and Mumper 2013). Utilising Human Serum Albumin (HSA) as a nanocarrier holds promise for preparing drug delivery systems and overcoming the solubility challenge (Zare and Makvandi 2019).

Currently, researchers have reported various methods for the preparation of protein-based nanoparticles (NPs), including emulsification, desolvation, thermal gelation, and self-assembly (Martínez-López *et al.* 2020). Reversible or irreversible aggregation of protein segments or non-covalent interactions such as van der Waals forces, hydrophobic interactions, electrostatic interactions, hydrogen bonding, and π–π stacking interactions can induce the self-assembly of proteins (Zare and Makvandi 2019, Varma *et al.* 2020). The characteristics of the resulting self-assembled structures depend on mechanical strength, pH, temperature,

---

ionic strength, and the type of ions present in the system (McManus *et al.* 2016).

HSA is the most abundant plasma protein (35–50 g/L of serum) in human blood (Kratz 2008). It is non-toxic, biodegradable, biocompatible, highly water-soluble, non-immunogenic, easy to purify, and stable in plasma (Elzoghby *et al.* 2012). It consists of 585 amino acid residues and has a molecular weight of 66.5 kDa (Rabbani and Ahn 2019). It exhibits an α-helix structure lacking β-sheets (Carter *et al.* 1989). Its three-dimensional structure, studied by X-ray crystallography, has three identical domains named I, II, and III (Rabbani and Ahn 2021). Each one consists of two subdomains A (4 α-helices) and B (6 α-helices) (Larsen *et al.* 2016), 17 disulphide bridges, and a free sulfhydryl group from a cysteine residue (Cys). Additionally, it features a unique tryptophan residue (Trp 214) and high amounts of glutamic acid (Glu), arginine (Arg), and lysine (Lys). HSA carries around 19 negative charges at pH 7.4 (Alvarez *et al.* 2010), due to the presence of more amino acid residues with acidic groups than amino groups (Elzoghby *et al.* 2012, Rabbani and Ahn 2019).

The structural and functional aspects of HSA can be understood in relation to the elucidation of the protein denaturation mechanism (Ptitsyn 1995). In this case, proteins can become less stable when small molecules like urea are present (chemical denaturation, CD) or when the temperature rises (thermal denaturation, TD) (Santoro and Bolen 1988). In CD, the urea disrupts the non-covalent interactions in the protein (Guckeisen *et al.* 2021), causing exposure of hydrophobic domains, making them available for interaction with lipophilic drugs and self-assembling into nanoparticles (Lin *et al.* 2016).

In TD, it has been observed that an increase in temperature above 50 °C leads to a reversible separation of domains I and II (Rabbani *et al.* 2017a). Conversely, at temperatures below 70 °C, domain II undergoes irreversible unfolding, whereas at temperatures equal to or exceeding 70 °C, domain I unfolds irreversibly (Flora *et al.* 1998). In both cases, the protein denaturation increases the hydrophobicity of the protein through exposing non-polar amino acid residues to a more polar environment (solvophobic effect) (Picó 1999).

This study examines the conformational changes induced by CD and TD on HSA at pH 7.4 and 9.9, as well as their influence on self-assembled NPs formation with PTX. The HSA interactions with urea and Tris solutions at pH 7.4 and 9.9 and comparisons of HSA physicochemical behaviour on the Phosphate Buffer System (PBS) will be explored by experimental and computational methods. The results will be useful for explaining the encapsulation and release efficiency of PTX from the HSA NPs made by self-assembly method.

2. Methods

2.1. Materials

Human Serum Albumin (lyophilised powder ≥97%w/w agarose gel electrophoresis, product code A9511Sigma-Aldrich), urea (ReagentPlus® ≥99.5%w/w product code U1250), sodium hydroxide (ACS reagent ≥97.0%w/w, pellets, product code 221465), fuming hydrochloric acid (ACS reagent, 37%w/v product code 258148), ethanol anhydrous (200 proof, anhydrous ≥99.5%v/v product code 459836) and sodium chloride (ACS reagent, ≥99.0% w/w, product code S9888) were all bought from Merck. Tris (hydroxymethyl) aminomethane for analysis ACS 99.8–100.1%w/w (Panreac, ITW Reagents product code 131940), deionised water (milliQ), monobasic sodium phosphate (ReagentPlus® ≥99.0% w/w, product code S0751), and sodium phosphate dibasic solution (ACS reagent ≥99.0% w/w, product code S9763) were purchased from Sigma Aldrich and Paclitaxel (99.92% w/w product code T0968, was purchased from TargetMol®).

2.2. Methods

2.2.1. Buffer solutions

The solutions prepared for TD: 0.16 M PBS ($\mu = 190$ mM) at pH 7.4 and 1 M Tris at pH 9.9. For CD: 1 M Tris/6 M Urea/0.3 mM $NaBH_4$ and adjusted at pH 7.4 or pH 9.9.

2.2.2. Denaturation of HSA

Each buffer solution is composed of 6.0 mg of HSA. The solutions obtained are incubated consecutively at temperatures of 25 and 50 °C (for CD), and at temperatures of 25 and 70 °C (for TD) for a duration of 30 min each. Ultimately, all samples are cooled to the ambient temperature and subjected to characterisation investigations in both solution and lyophilised stages.

2.2.3. HSA-PTX NPs preparation

After the HSA has been denatured and cooled to room temperature (CD and TD), it is stirred using a magnetic stirrer at a speed of 500 rpm. Then, 40 μL of PTX (800 μg) is slowly added in small drops from a stock solution with a concentration of 20 mg/mL dissolved in ethanol. Afterward, 1.260 μL of deionised water is added. Subsequently, the mixture is allowed to stir for a duration of 4 h. Following this, the HSA-PTX NPs

synthesised on Tris and Tris/Urea are rinsed to achieve a neutral pH using Amicon® centrifugal ultrafiltration tubes with a 50 kDa cut-off at a speed of 7.780 rpm.

2.3. Experiments

2.3.1. Differential scanning calorimetry (DSC)

To analyse the thermal transitions of HSA in each buffer, the samples are dehydrated using a LABCONCO FreeZone Plus 6 lyophilizer set at a temperature of $-88 ℃$ and kept at a vacuum level of 0.144 mbar for a duration of 24 h. The analytical process utilises a TA Instruments Q100 DSC equipment, which employs perforated aluminium hermetic capsules. The analysis consists of a controlled scan, beginning with a constant temperature of 0 ℃ maintained for 5 min, followed by a gradual increase in temperature of 1 ℃/min until reaching 100 ℃ in an N_2 environment. The heat data (expressed in W/g) is then analysed and interpreted using the TA Instruments Universal Analysis 2000 Software.

2.3.2. UV-Vis spectroscopy

The UV-Vis absorption spectra of HSA in each buffer are measured using UV-Vis spectroscopy on a Perkin Elmer Lambda 35 UV/Vis spectrophotometer equipped with UV Winlab software. The spectra range from 200 to 350 nm. The UV-Vis spectra are measured at both ambient temperature and following the application of the suitable CD or TD treatment. Duplicate analyses are conducted for each sample.

2.3.3. Intrinsic fluorescence spectroscopy

After dissolving HSA in each buffer solution, intrinsic fluorescence spectroscopy is conducted. Fluorescence spectra are obtained at ambient temperature and following the appropriate thermal treatment. To do this, a volume of 100 μL of the sample is introduced onto 96-well plates. The plates are then stimulated at a wavelength of 280 nm, and the resulting emission spectra data is recorded from 300 to 600 nm using a Varioskan LUX microplate reader equipped with SkanIt Microplate Readers RE Software. Blank signals are subtracted, and duplicate analyses are conducted.

2.3.4. Mean diameter and size distribution

Mean diameter distribution of HSA and HSA-PTX NPs, respectively, are measured by dynamic light scattering (DLS) on HORIBA LB 550 equipment (Kyoto, Japan). Measurements of the HSA and HSA-PTX NPs dispersed in each buffer system are carried out at 25 ℃. The measurements are performed in triplicate.

2.3.5. ζ-Potential

ζ-Potential determinations are carried out using a Malvern Zetasizer (Nano series) at room temperature with a 1:10 dilution in deionised water of each system. Each sample is analysed by triplicate.

2.3.6. Paclitaxel quantification

Encapsulation efficiency (EE) of PTX in the HSA-PTX NPs is quantified using HPLC with a Liquid Chromatograph System (Waters™) equipped with a Waters 2489 UV/Vis detector. A Phenomenex Luna 5 μm C18 column (250×4.6 mm × 5.0 μm) is employed, maintained at 25 ℃ throughout the analysis. The mobile phase is an isocratic mixture of ACN:H_2O (70:30), with a flow rate of 0.8 ml/min. A 20 μL volume of sample is injected, and the analysis duration is 10 min. Detection is performed at a wavelength of 228 nm (Thao *et al.* 2017). A calibration curve of PTX in an ACN:Buffer mixture (90:10) is made, ranging from 3.9 μg/mL to 250.0 μg/mL with seven points. The calibration curve is evaluated through linear regression and plot the area against PTX concentration. The characteristic parameters of the regression are obtained using the least-squares method. The calibration curve demonstrated linearity, with a correlation coefficient $R=0.999998$ and a coefficient of determination $R^2=99.9997\%$. The EE is determined by triplicate and according to Wimalasiri *et al.* (2021).

2.3.7. In vitro PTX release

The *in vitro* release profile of PTX from HSA NPs is assessed using the dialysis method with a PBS buffer at pH 7.4 as the release medium. The HSA-PTX NPs prepared by using CD of HSA at pH 7.4 and 9.9, as well as TD at pH 9.9, are purified using Amicon® centrifugal ultrafiltration tubes with cut-off size of 50 kDa, at a centrifugation speed of 7.780 rpm and until reaching a neutral pH value. The NPs obtained with TD of HSA at pH 7.4 are used without additional purification. Subsequently, each of these systems is loaded into a Float-A-Lyzer® dialysis tubes (MWCO 20 kDa) (Spectrum Labs). The tubes are suspended in the release medium at 37 ℃, which is maintained under magnetic stirring at 100 rpm. One hundred microlitres of aliquots are withdrawn from the dialysis tube and replenished with the same volume of fresh medium. This experiment is conducted by triplicate and reported as mean ± s.d. (Hasanbegloo *et al.* 2023).

2.3.8. Protein docking

The tridimensional structure of PTX and HSA are downloaded from the protein data bank (PDB codes: TA1 and 1AO6, respectively). The structures are prepared (side chains completing, water deleting, and hydrogen/charge adding) on Chimaera 1.17 Software. The docking analysis is carried out on the primary, secondary, and site 3 binding sites of PTX on HSA (Paal *et al.* 2007, Wang *et al.* 2013, Salem *et al.* 2019) keeping the box size equal to $(30\,\text{Å})^3$, is used to ensure extensive ligand binding coverage, considering that one the most commonly used grid box size for HSA is $(25\,\text{Å})^3$ (Ferrari and Patrizio 2021). The scoring is made with Autodock Vina and visualisation of the results on Chimaera 1.17 program.

The electrostatic potential maps of the protein at pH 7.4 and 9.9 are calculated on https://server.poissonbo ltzmann.org/pdb2pqr server and depicted by using Pymol visualiser. The ζ-potential curves calculated from the number and ionisation degree of ionisable aminoacids of the protein (Moore 1985).

The Protein Interfaces Surface Analysis (PISA) for evaluating the energy involved in the formation of stable protein quaternary structures is made at https://www.ebi.ac.uk/msd-srv/prot_int/cgi-bin/piserver.

2.3.9. Statistical analysis

UV-Vis and fluorescence studies are assessed by duplicate ($n=2$) and analysed using Pearson correlation analysis (r), establishing a linear relationship between two continuous variables. Significant correlation is established by the values $0.6 < r < 0.79$ as high correlation and $0.8 < r < 1.0$ as very high correlation (Almashhadani *et al.* 2023). In triplicate experiments ($n=3$), statistical analysis is performed using ANOVA or Kruskal–Wallis, based on data number or behaviour, using Statgraphics Centurion XVI software with a 95% confidence level. Significant statistical differences are found when $p < 0.05$. The Kolmogorov–Smirnov and Levene tests also tested normality and homocedasticity.

3. Results and discussion

The thermal or chemical denaturation of HSA exposes its hydrophobic core, allowing drugs to be incorporated into pharmaceutical delivery systems (Hoogenboezem and Duvall 2018). Under buffered conditions, HSA-drug self-assembly can produce stable formulations. The specific interacting pH controls the chemical environment of the protein and optimum drug binding (Rabbani *et al.* 2017b, 2018). This study will explore the HSA interactions with urea and Tris solutions at pH 7.4 and 9.9, utilising both experimental and computational methods, and drawing comparisons with PBS. We will then use these interactions to explain the role of PTX incorporation as a proof concept.

3.1. Human serum albumin denaturation on PBS and Tris buffers

After lyophilisation, DSC follows the TD of HSA on PBS at pH 7.4. The phosphate ions protect the protein under freezing-drying conditions (Izutsu *et al.* 2009). This is because these ions cross-link proteins through electrostatic interactions with lysine (Lys), histidine (His), and arginine (Arg) residues, hydrogen bonds, and sulfhydryl groups that keep the protein stable (Akahane 1982). The DSC thermogram of HSA-PBS pH 7.4 after heating at 1 °C/min presents three endothermic, non-reversible events (Figure 1(a)). This can be correlated with partially (42 and 50 °C) and fully (70 °C) unfolded protein molecule populations. The first population around 40 °C is also observed in Tris/urea pH 7.4 (Figure 1(b)), but the protein is fully unfolded at the lowest temperature than in PBS pH 7.4. This is the CD effect on amides, where urea can shift the water molecules of the protein structure. This occurs primarily via hydrogen bonds and other electrostatic interactions with charged and polar side chains (Hua *et al.* 2008). The protein is less stable to TD and CD at pH 9.9 on Tris and Tris/urea (Figures 1(c,d)). The HSA exhibits a higher negative density at this high pH, leading to the easy denature of its basic form due to electrostatic repulsions (Shaw and Pal 2008, Baler *et al.* 2014).

Considering these DSC results, spectroscopic techniques at 50 and 70 °C corroborate the stability of the HSA 3D structure in different buffers and pHs. The UV spectra of HSA-PBS buffer at pH 7.4 exhibit the maximum absorption around 280 nm. The Edelhoch equation (Equation (1) describes the contributions of Trp, tyrosine (Tyr), and cystine (disulphide bonds) to the molar extinction coefficient (ε280) (Pace *et al.* 1995, Batabyal *et al.* 2021). The phenylalanine (Phe) also contributes to the spectra, mainly at wavelengths smaller than 270 nm.

$$\varepsilon_{280} = 5500 * 1uA_{(Trp)} + 1490 * 18uA_{(Tyr)} + 125 * 17uA_{(Cystine)}$$
$$= 34445 M^{-1} cm^{-1} \tag{1}$$

The wavelength of these bands is similar at 25, 50, and 70 °C, independent of the buffer and pH (Figures 2(a–c)). At the tested temperatures, there is no significant difference in absorption band intensity between the HSA-PBS 7.4 and HSA-Tris 9.9 (Table 1). However,
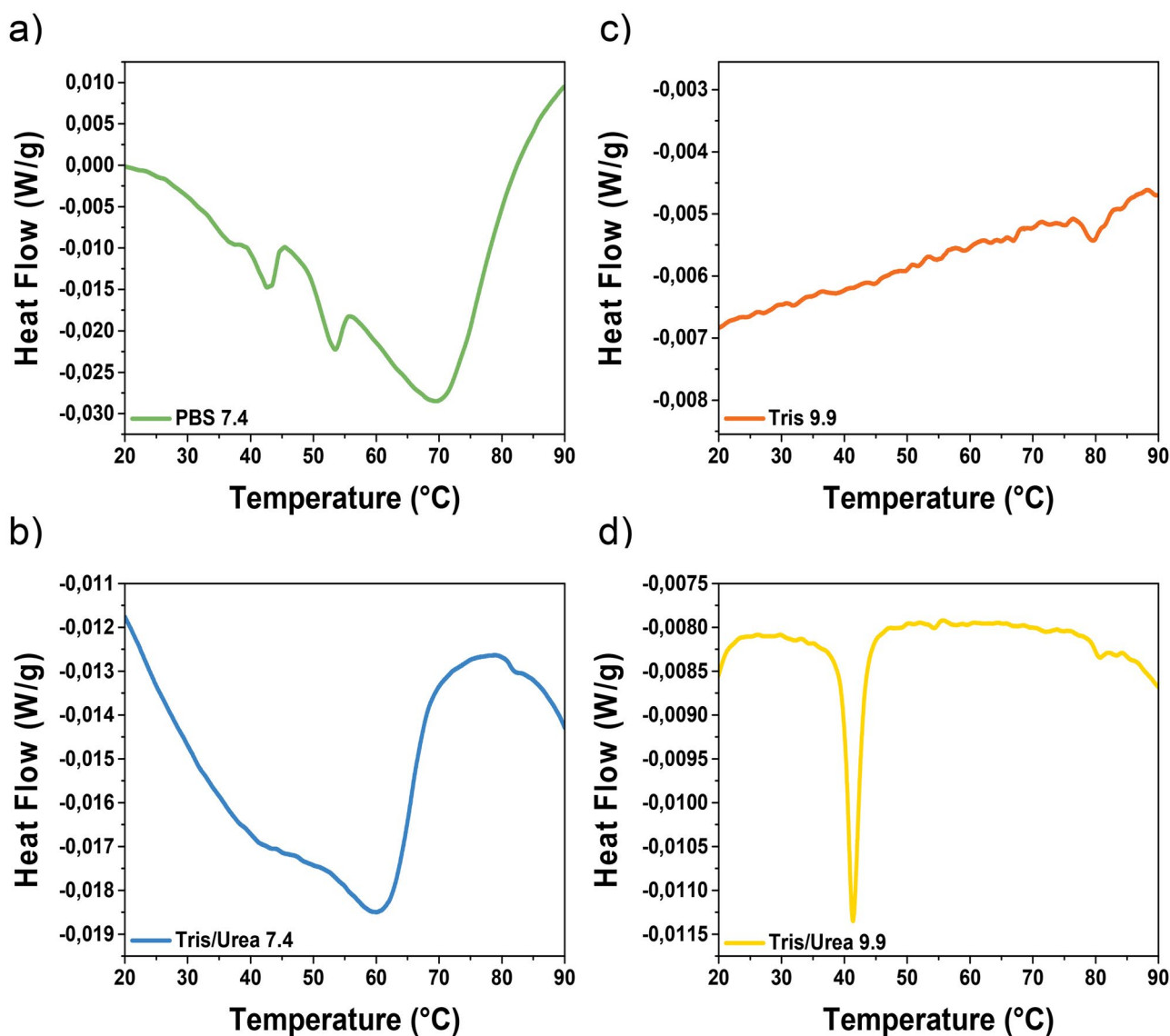
Figure 1. Differential scanning calorimetry (DSC) thermograms for lyophilised human serum albumin (HSA) samples at pH 7.4 and 9.9 on different buffers. (a) HSA-PBS (phosphate buffer saline) pH 7.4 presents three endothermic non-reversible events, they can be correlated with partially (42 and 50 °C) and fully (70 °C) denatured protein molecule populations. (b) HSA-Tris/urea pH 7.4 presents the first population around 40 °C is also observed, but HSA is fully denatured at lowest temperatures than in PBS pH 7.4. (c,d) At pH 9.9, the HSA has a higher negative density, and the basic form of this protein can be easily denatured as consequence of electrostatic repulsions.

the absorbance decreases significantly in the presence of urea, being most important at 50 and 70 °C in Tris buffer at pH 9.9. Considering that all HSA dispersions are prepared with a concentration equal to 6 mg/mL, these differences in absorption intensity at 280 nm can be attributed mainly to changes in the Tyr and Trp chemical environments. This is supported by the hypochromic effect of $\sim$310 ± 5 nm on the fluorescence spectra (λ_{ex} = 280 nm at 25 °C) for HSA Tris/urea pH 9.9 dispersion heated at 50 °C, Tris pH 9.9, and Tris/urea pH 9.9 at 70 °C (Figures 2(d–f) and Table 2). The presence of Tris and urea, in addition to the high negative charge density of HSA at this pH, affects the protein

shape, charged groups, and water molecules near Trp and Tyr (Vivian and Callis 2001, Möller and Denicola 2002, Chilom et al. 2007). DSC correlates the non-reversible full denaturation at 70 °C and pH 9.9 with thermal conformational changes, partial denaturation, and chemical quenching (Figure 1).

The partial and full denaturation favour the exposition of hydrophobic aminoacids to the water. This promotes the intermolecular protein interactions, which explains the agglomerates detected by DLS. These appear especially at 70 °C (Table 3). The solvophobic effects explain the molten globule and aggregation states of unfolded HSA under thermal
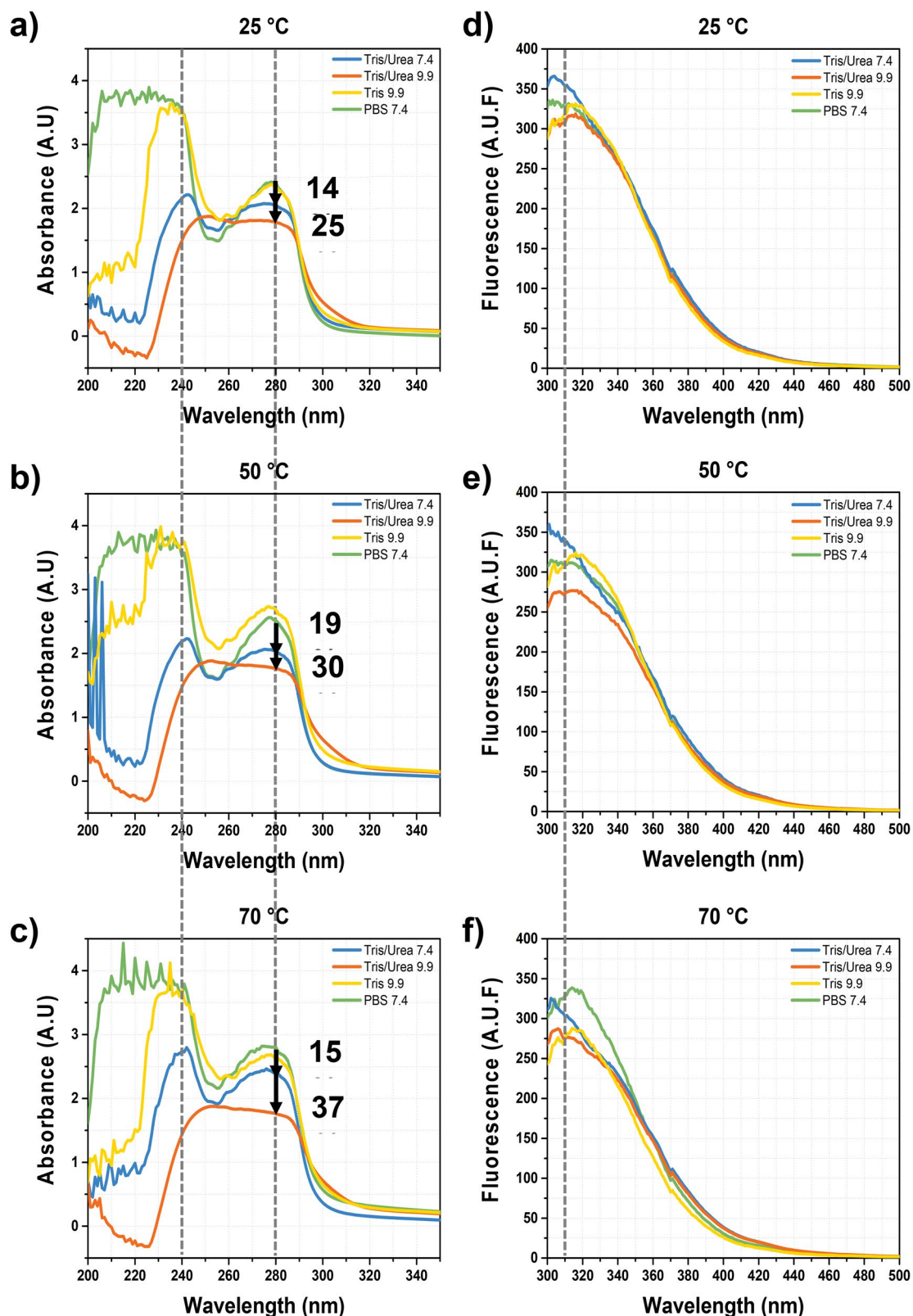
Figure 2. UV-Vis and intrinsic fluorescence spectra of human serum albumin (HSA), showing maximum absorption around 280 nm and fluorescence emission at 310 nm. (a,d) Depict HSA at 25 °C, (b,e) show HSA at 50 °C, and (c,f) illustrate HSA at 70 °C. For the absorption spectra, the maximum absorbance wavelengths are similar at 25, 50, and 70 °C, regardless of the buffer and pH. The differences on the absorption intensity at 280 nm can be described mainly to changes on the tyrosine (Tyr) and triptophane (Trp) chemical environment. There is no difference in band intensity between HSA-PBS pH 7.4 and HSA-Tris pH 9.9 samples at the evaluated temperatures ($p > 0.05$). However, in the presence of urea, the absorbance decreases significantly, with the most notable reductions occurring at 50 and 70 °C, by 30 and 37% respectively, in Tris buffer at pH 9.9. Fluorescence spectra (d–f) HSA exhibits a hypsochromic shift to a lower wavelength in the same buffer system.

Table 1. Absorbance values at 280 nm for human serum albumin (HSA) in different buffers at 25, 50, and 70 °C.

HSA	Absorbance[a] (A.U) 25 °C	Pearson correlation coefficient, r	Absorbance[a] (A.U) 50 °C	Pearson correlation coefficient, r	Absorbance[a] (A.U) 70 °C	Pearson correlation coefficient, r
PBS pH 7.4	2.3893 ± 0.0914	0.9923	2.5214 ± 0.0262	0.9983	2.8027 ± 0.0307	0.9960
Tris/urea pH 7.4	2.0528 ± 0.2011	0.9883	2.0384 ± 0.2287	0.6818	2.3768 ± 0.2015	0.9287
Tris/urea pH 9.9	1.7804 ± 0.0696	0.9951	1.7620 ± 0.0639	0.9976	1.7604 ± 0.0154	0.9989
Tris pH 9.9	2.3494 ± 0.3217	0.9875	2.6874 ± 0.1324	0.8156	2.6183 ± 0.0104	0.9955

[a]The data are presented as mean ± s.d. ($n = 2$). Human serum albumin (HSA) in each buffer. Phosphate buffer saline (PBS), standard deviation (s.d.). Arbitrary units (A.U). Pearson correlation (r) analysis was performed on all absorbance data to establish the linear relationship between two continuous variables. Despite the small sample size ($n = 2$), all data show good correlation, validating the results.

Table 2. Fluorescence values at 310 nm for human serum albumin (HSA) in different buffers at 25, 50, and 70 °C.

HSA	F (A.U.F)[a] 310 nm, 25 °C	Pearson correlation coefficient, r	F (A.U.F)[a] 310 nm, 50 °C	Pearson correlation coefficient, r	F (A.U.F)[a] 310 nm, 70 °C	Pearson correlation coefficient, r
PBS pH 7.4	328.3 ± 16.9	0.9995	310.9 ± 11.3	0.9998	329.0 ± 29.6	0.9997
Tris/urea pH 7.4	353.6 ± 11.7	0.9999	335.5 ± 1.0	0.9997	302.6 ± 2.9	1.0000
Tris/urea pH 9.9	306.6 ± 18.8	0.9999	273.1 ± 19.8	0.9996	274.9 ± 6.6	1.0000
Tris pH 9.9	318.9 ± 6.4	0.9998	309.7 ± 1.9	1.0000	275.4 ± 0.4	0.9997

[a]The data are presented as mean ± s.d. ($n = 2$). Human serum albumin (HSA) in each buffer. Phosphate buffer saline (PBS), standard deviation (s.d.). Arbitrary units of fluorescence (A.U.F). Pearson correlation (r) analysis was performed on all fluorescence data (Almashhadani et al. 2023). All data show very high correlation.

Table 3. Mean diameter values for human serum albumin (HSA) in different buffers at 25, 50, and 70 °C, obtained after consecutive incubation at temperatures of 25, 25, and 50 °C for chemical denaturation (CD), and 25 and 70 °C for thermal denaturation (TD) for a duration of 30 min each.

HSA	Mean diameter (nm) 25 °C[a]	50 °C[a]	70 °C[a]
PBS pH 7.4	14.9 ± 3.4	14.6 ± 0.7	48.5 ± 5.3
Tris/urea pH 7.4	15.8 ± 5.3	14.3 ± 4.7	51.2 ± 2.5
Tris/urea pH 9.9	142.5 ± 79.3*	16.7 ± 1.9	32.7 ± 17.0
Tris pH 9.9	14.6 ± 1.8	15.4 ± 2.4	19.5 ± 5.7*

The measurements are conducted when each system reaches room temperature.
*Indicates data with significant differences ($p < 0.05$), assessed using one-way analysis of variance (ANOVA) and the Kolmogorov–Smirnov test, comparing temperature groups. Statistical differences at 25 °C in the mean diameter of HSA in Tris/urea pH 9.9 suggest that the electrostatic environment with the urea induces aggregation states of folded HSA. However, in Tris pH 9.9 after TD at 70 °C (19.5 ± 5.7 nm), the mean diameter is smaller than in the other systems, indicating that intermolecular repulsions due to the increased electrostatic charge on the molecular surface of HSA may contribute to maintaining the monomeric forms at pH 9.9 in the absence of urea.
[a]Data are presented as mean ± s.d. ($n = 3$). Human serum albumin (HSA) in each buffer.

treatment. In the case of CD with urea, the electrostatic environment of exposed residues has been also considered (Farruggia and Picó 1999). The PBS protects the albumin against chemical denaturation more than Tris buffer (Tayyab et al. 2022). However, the average mean diameter on Tris 9.9 (19.5 ± 5.7 nm) is smaller than on PBS 7.4 (48.5 ± 5.3 nm), with significant statistical differences, $p < 0.05$ (Table 3). This makes to think, that intermolecular repulsions for the increased electrostatic charge on the molecular surface of the HSA can contribute to maintain the monomeric forms at pH 9.9 in the absence of urea (Farruggia and Picó 1999).

3.2. Human serum albumin—paclitaxel NPs

The TD and CD demonstrated in the precedent section are implemented for producing HSA-PTX NPs.

Heating at 70 °C during the TD of HSA-PBS 7.4 and HSA-Tris 9.9 increases the mean diameter of HSA (Table 3). Following the TD treatment of HSA, PTX loading and the self-assembly of NPs occur at 25 °C. The NPs prepared in Tris at pH 9.9 are smaller than ones in PBS at pH 7.4, with significant differences ($p < 0.05$); nevertheless, the PDI and ζ-potential values, have no significant differences, $p > 0.05$ (Table 4).

The PTX loading, or EE, of the NPs prepared by TD yields results of 96.4 ± 2.1% w/w for pH 7.4 and 97.3 ± 0.2% w/w for pH 9.9. There are no statistically significant differences ($p > 0.05$), and these values are consistent with the reported range of 89–98% for PTX bound to plasma (Rowinsky 1997). However, PTX is looser bound on the HSA-PTX systems prepared by TD at pH 9.9 than at pH 7.4. The former NPs release a higher percentage of PTX within 1 h, keeping only about 30% after 1 h of contact with a PBS solution at 37 °C (Table 4), but in contrast to the HSA-PTX NPs prepared in PBS pH 7.4, ~60% of PTX remains. This suggests that the PTX binding strength is higher on the HSA-PTX NPs unfolded in PBS pH 7.4 than in Tris pH 9.9.

At 50 °C, urea induces the CD in Tris at pH 7.4 or 9.9. After that, the PTX loading at 25 °C does not avoid the agglomeration with a mean diameter for the NPs for Tris/urea pH 7.4 and Tris/urea pH 9.9, respectively, leading to a high PDI on HSA-PTX NPs prepared with Tris/urea pH 9.9 ($p < 0.05$) (Table 4). EE was lower for HSA-PTX NPs made at pH 7.4 by CD of HSA compared

to EE achieved by TD. This is because HSA and PTX did not interact well, which could be because HSA was not fully open at the urea concentration used (González-Jiménez and Cortijo 2002). Mean diameter of HSA-PTX NPs made at pH 9.9 by CD is very different from NPs made at the same pH by TD ($p < 0.05$). The γ-potential does not show any statistical differences ($p > 0.05$) and is a measure of how stable NPs are in physiological conditions.

In relation to *in vitro* release, these NPs prepared by CD of HSA demonstrate the release of up to 50% of PTX in 1 h, following the washing step to introduce them into a physiological medium, with <50% remaining as residual content (Table 4).

In summary, the choice of the TD or CD pathway affects the EE. The PTX binding strength depends on the buffer type and pH, even in the presence of urea. This encourages the study of the impact of the protein environment (electrostatics, hydrophobicity) and the nature of the buffer on the modulation of the HSA-PTX interactions.

Accordingly to Figure 3, this displays the electrostatic surface potential maps of the monomeric and dimeric HSA at pH 7.4 and 9.9 above its isolectric point (Gianazza *et al.* 1984, Turell *et al.* 2014). The monomeric form is in its native state at pH 7.4 and is highly stabilised by the negative charge of the phosphate ions on PBS, as demonstrated experimentally.

Table 4. Characteristics of the self-assembled human serum albumin (HSA) nanoparticles (NPs) containing paclitaxel (PTX).

NPs system	Mean diameter[a] (nm)	PDI[a]	ζ-potential[a] (mV)	EE[a] (% w/w)	PTX Release in 1 h[a] at 37 °C
HSA-PTX PBS pH 7.4	287.1 ± 12.9*	0.10 ± 0.01	−36.5 ± 1.4	96.4 ± 2.1	37.7 ± 7.2*
HSA-PTX Tris pH 9.9	191.5 ± 9.2*	0.08 ± 0.02	−40.3 ± 7.9	97.3 ± 0.2	68.7 ± 14.0
HSA-PTX Tris/urea pH 7.4	584.2 ± 47.7*	0.08 ± 0.01	−36.5 ± 9.8	75.9 ± 4.9*	52.5 ± 14.1
HSA-PTX Tris/urea pH 9.9	406.2 ± 28.1*	0.15 ± 0.02*	−30.6 ± 5.2	92.9 ± 1.6	60.2 ± 11.3

PDI: polydispersity index; EE: encapsulation efficiency.
The NPs prepared by the thermal denaturation (TD): phosphate buffer saline (PBS) and Tris pH 7.4 and 9.9, respectively, and chemical denaturation (CD): Tris/urea pH 7.4 and 9.9, respectively. The self-assembly of the NPs with PTX is performed at room temperature.
*Data were significantly different ($p < 0.05$). It was assessed by one-way analysis of variance (ANOVA) through Kolmogorov-Smirnov test.
[a]Data show mean ± s.d. ($n = 3$). Nanoparticles (NPs) of human serum albumin (HSA) self-assembled with paclitaxel (PTX).
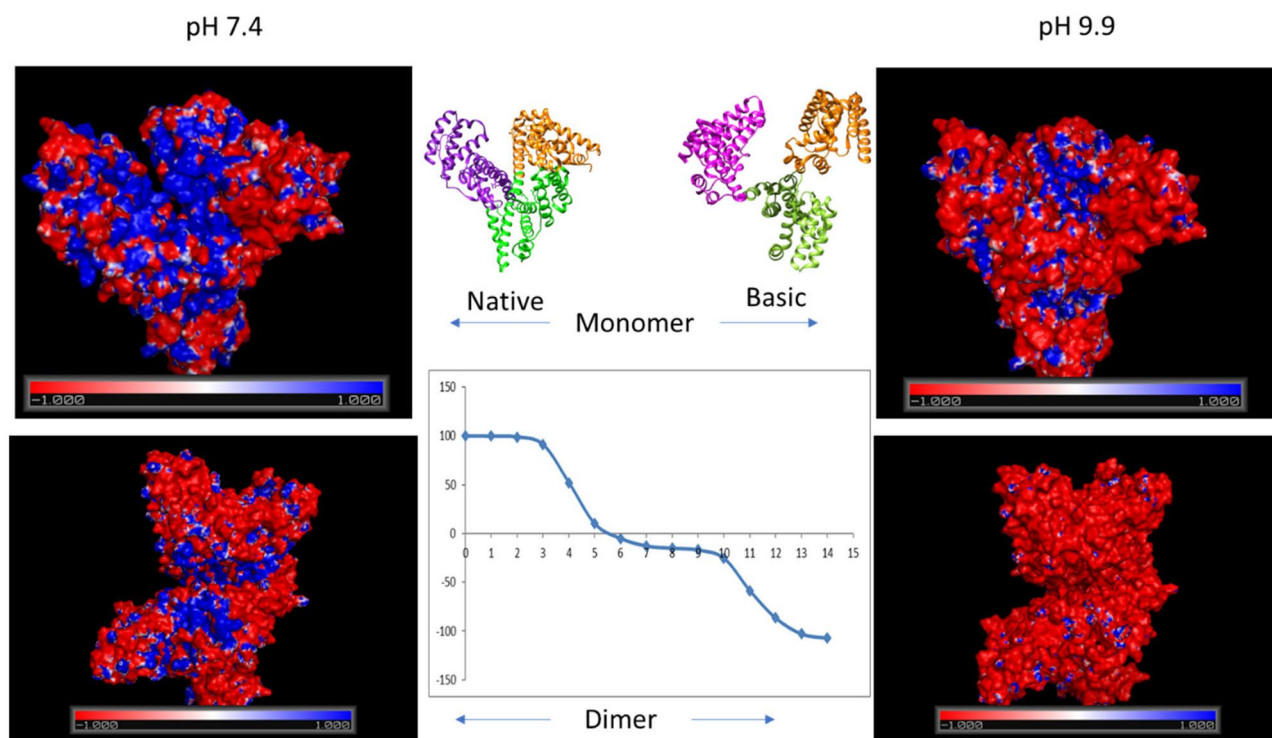

Figure 3. Calculated ζ-Potential curve and electrostatic surface potential maps at pH 7.4 and 9.9 for human serum albumin (HSA) monomer (above) and dimer (below) forms. The monomeric form is in the native state at pH 7.4 and highly stabilised by the negative charge of the phosphate ions on phosphate buffer saline (PBS), as shown experimentally. The negative density charge increases at pH 9.9 and this basic form is partially unfolded. This contributes to the HSA thermal denaturation (TD) and chemical denaturation (CD) observed on Tris at pH 9.9.

At pH 9.9, the negative density charge rises, leading to a partial unfolding of this basic form (Baler *et al.* 2014). This contributes to the HSA TD and CD observed on Tris at pH 9.9 (Figures 1(c,d)). So, PTX might be easier to deliver from HSA-PTX NPs made by heating HSA at pH 9.9 on Tris than at pH 7.4 on PBS buffer (Table 4).

The HSA-PTX interactions can also be analysed within the hydrophobic environment of HSA, which is enhanced by the weakening of thermal denaturation process (Ahmad *et al.* 2012). The PTX is a diterpene exhibiting a baccatine core (taxane, oxetane rings) and an ester chain (Mastropaolo *et al.* 1995). This chemical structure has 4 hydrogen bond donors, 14 hydrogen bond acceptors, and 14 rotable bonds (PubChem Data) with a dipolar moment ($m = 10.732508\,D$). Its electrostatic surface potential map and logP = 2.5 indicate its lipophilic character (Figure 4). This makes it more likely that it will interact with the HSA on the Sudlow I, or primary binding site, which is where the IIA and IIIA subdomains meet (Figure 4). Our docking analysis in Sudlow I corroborates that the ester chain is buried in the IIA subdomain, with stabilised H-bonds and Van der Waals interactions with Lys199, His242, Arg222, and Arg218 residues. Meanwhile, the rigid baccattin core is moving towards the IIIA one, as reported by experimental and docking studies (Paal *et al.* 2007).

The PTX docking study also corroborates the interactions on the secondary binding site (cleft formed between I and III domains) of HSA reported in the literature (Wang *et al.* 2013, Salem *et al.* 2019). Even though Sudlow II is the weakest PTX binding site, the affinity of Tris and urea molecules for HSA is very similar to that of the primary and secondary binding sites (Figure 5). Therefore, both Tris and urea molecules can be well-distributed along the HSA molecule. The comparison with Tris and urea interaction energies demonstrates that these buffers do not compete with PTX. This is because a larger molecule has a higher affinity than a smaller one. However, the scaling affinity by molecular size indicates that urea exhibits the highest ligand efficiency (LE = docking score/number of heavy atoms) compared to Tris and PTX. This helps to explain the chemical denaturation effect of the urea (Hua *et al.* 2008). However, the interactions between Tris or urea and the PTX ester chain, which can be seen on the primary and secondary HSA binding sites, can change the affinity between PTX and HSA. This is one reason why HSA-PTX NPs Tris 9.9 and Tris/urea 7.4 and 9.9 delivered more PTX than PBS 7.4 after 1 h.
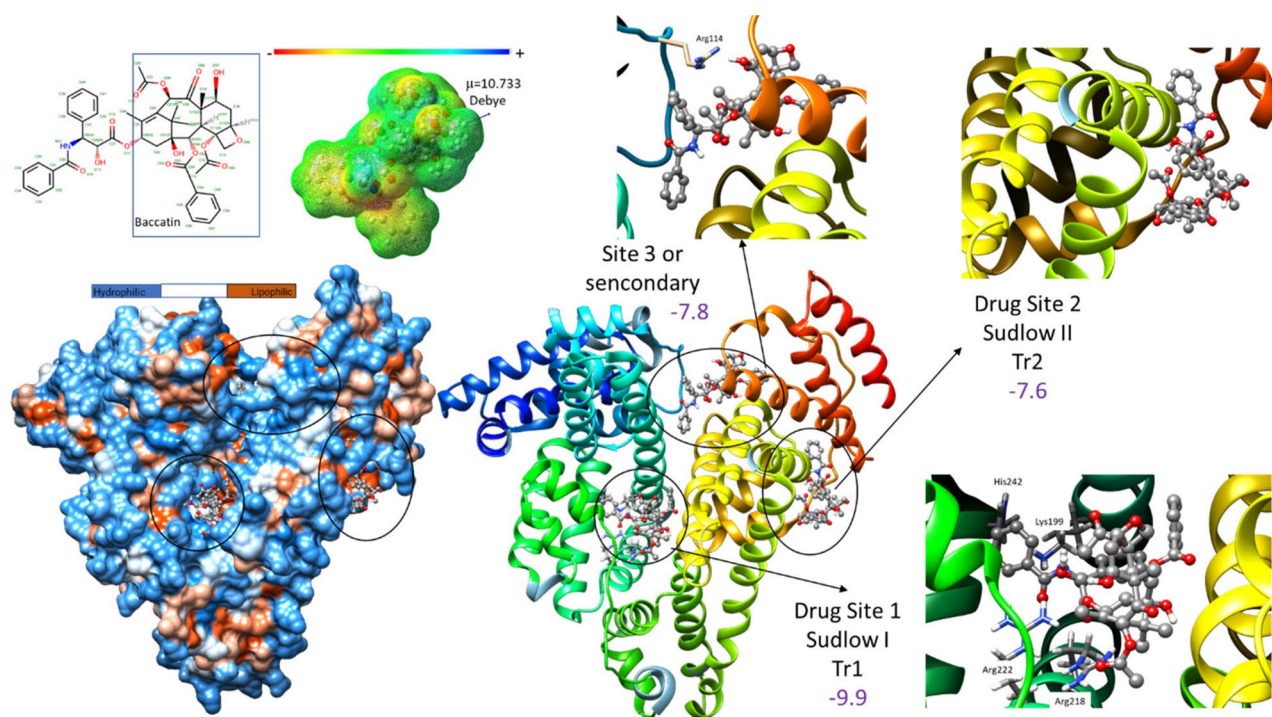
Figure 4. Chemical structure, electrostatic potential map and docking results of paclitaxel (PTX) on drug interactions sites of the human serum albumin (HSA), shown on the hydrophobicity surface map and ribbons representations of this protein. The magenta numbers indicate the PTX-HSA interaction energy in kcal mol^{-1}. The ester chain is buried in the IIA subdomain, stabilised H-bonds and Van der Waals interactions with Lysine199 (Lys199), Histidine (His242), Arginine222 (Arg222), and Arginine218 (Arg218) residues.
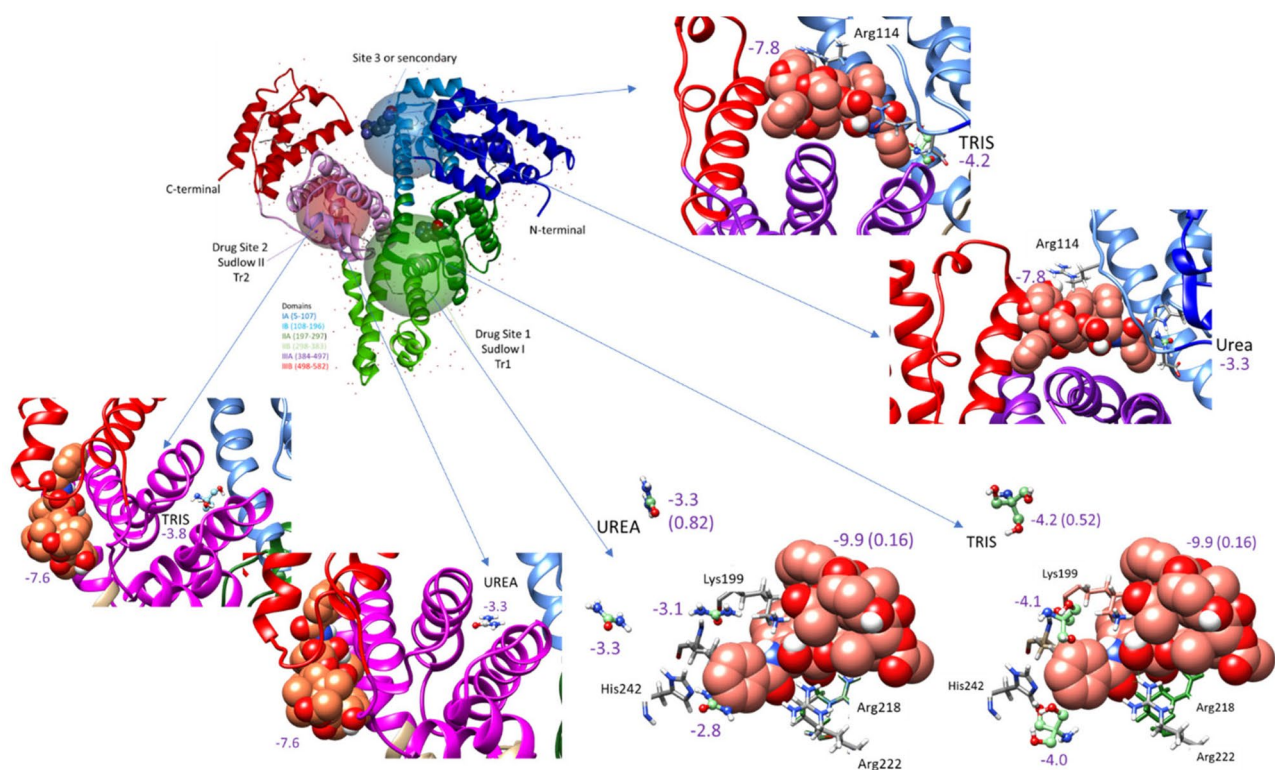
Figure 5. Interactions of paclitaxel (PTX) (spheres) and Tris or urea (ball and sticks) in the primary (Sudlow I), secondary and Sudlow II sites of Human Serum Albumin (HSA). The magenta numbers indicate the interaction energy in kcal mol⁻¹ and in parenthesis the ligand efficiency (LE). The Sudlow II is the weakest PTX binding site, the affinity of Tris and urea molecules for HSA is very similar than in the primary and secondary binding sites.

Table 5. The protein interfaces surface analysis (PISA) for evaluating the energy involved on the formation of stable protein quaternary structures.

Structure 1			Structure 2					Interface	Δ_iG				
Range	^{i}Nres	Surface (Å²)	Range	Symmetry op-n	Sym.ID	^{i}Nres	Surface (Å²)	Area (Å²)	kcal/mol	N_{HB}	N_{SB}	N_{DS}	CSS
B	20	27 347	A	x, y, z	1_555	23	27 936	439.8	−4.3	4	3	0	0.000
B	17	27 347	B	x−1, y, z	1_455	19	27 347	327.4	2.1	4	4	0	0.000
A	18	27 936	A	x, y, z−1	1_554	14	27 936	230.3	−0.2	2	2	0	0.000
A	14	27 936	B	−x+1, y−1/2, −z+1	2_646	15	27 347	260.0	0.1	1	0	0	0.000
B	12	27 347	B	x, y, z−1	1_554	12	27 347	210.7	−2.5	0	0	0	0.000
A	11	27 936	A	x−1, y, z	1_455	10	27 936	155.8	−2.2	0	0	0	0.000
[PO4]B:801	1	190	B	x, y, z	1_555	8	27 347	132.1	−5.7	2	0	0	0.029
[PO4]A:801	1	192	A	x, y, z	1_555	8	27 936	129.6	−6.7	2	0	0	0.032
A	1	27 936	B	−x+1, y−1/2, −z	2_645	1	27 347	18.1	−0.2	0	0	0	0.000
B	1	27 347	A	x−1, y, z	1_455	1	27 936	15.0	0.3	0	0	0	0.000
B	1	27 347	B	x−1, y, z−1	1_454	1	27 347	7.7	0.0	0	0	0	0.000
A	1	27 936	A	x−1, y, z−1	1_454	1	27 936	3.9	0.0	0	0	0	0.000

Sym. op-n: symmetry op-n indicates the symmetry operation that should be applied to 2nd interfacing structure to obtain the respective interface; ^{i}Nres: innovative non-redundant residues indicates the number of interfacing residues in the corresponding structure; N_{HB}=4: number of potential hydrogen bonds; N_{SB}=3: number of potential salt bridges; N_{DS}: number of potential disulphide bonds across the interface (Protein Data Bank in Europe 2024). Calculations are made in https://www.ebi.ac.uk/msd-srv/prot_int/cgi-bin/piserver.

3.3. Role of the intermolecular interactions on the NPs properties

Electrostatic, hydrophobic, van Der Waals, and H-bonds can mediate HSA intermolecular interactions (Ahmad *et al.* 2012). We conducted the PISA analysis by taking into account the number of residues on the interface, whose accessible surface could potentially contribute to the interface formation following the application of the specified symmetry operation on the second structure (Krissinel and Henrick 2007). The negative value of solvation-free energy gained when the interface formed (ΔiG=−4.3 kcal mol⁻¹) for the interchain interface with the largest area (439.8 Å²) shows that this is mainly hydrophobic (Table 5). This explains the agglomerates seen by

DLS, especially at 25 °C (Table 3). However, the electrostatic interactions must not be neglected. The repulsions are more expected at pH 9.9 than at 7.4 (Figure 4), which can correlate with the smaller mean diameter at Tris 9.9 (Table 3).

The number of potential hydrogen bonds ($N_{HB}=4$) and salt bridges ($N_{SB}=3$) across the interface is insufficient to stabilise stable HSA quaternary assemblies (Complexation Significance Score, CSS = 0) (Table 5). However, the presence of PTX, especially on Sites II and III, could improve these interactions, as evidenced by the increased mean diameter of HSA-PTX NPs (Table 3). The internal dynamics of the protein are influenced by ligand interactions, which in turn affects the energetics of protein–ligand associations (Ahmad *et al.* 2011), suggesting that PTX binding play a significant role in stabilising the assembly.

4. Conclusion

The choice of buffer and pH have a significant effect on the NPs properties, with PBS providing better stability at pH 7.4, while Tris buffers at higher pH level promote smaller mean diameters and rapid PTX delivery. Protein docking studies revealed insights into the conformational changes of HSA under the studied conditions, enhancing the understanding of NP formation. The results demonstrate that TD at pH 7.4 in PBS buffer creates the most favourable conditions for producing stable and efficient self-assembled HSA-PTX NPs with high EE and controlled drug release. These findings suggest that manipulating the denaturation process and buffer conditions can optimise HSA-based drug NPs for drug delivery systems.

Disclosure statement

No potential conflict of interest was reported by the author(s).

References

Ahmad, E., *et al.*, 2011. Stereo-selectivity of human serum albumin to enantiomeric and isoelectronic pollutants dissected by spectroscopy, calorimetry and bioinformatics. *PLOS one*, 6 (11), e26186. doi: 10.1371/journal.pone.0026186.

Ahmad, E., *et al.*, 2012. Pollutant-induced modulation in conformation and β-lactamase activity of human serum albumin. *PLOS one*, 7 (6), e38372. doi: 10.1371/journal.pone.0038372.

Akahane, T., 1982. *Freeze denaturation of fish muscle proteins*. Tokyo: Sophia University.

Almashhadani, M., *et al.*, 2023. Challenges in agile software maintenance for local and global development: an empirical assessment. *Information*, 14 (5), 261. doi: 10.3390/info14050261.

Alvarez, B., *et al.*, 2010. Chapter 5 – Formation and reactions of sulfenic acid in human serum albumin. *In*: E. Cadenas and L. Packer, eds. *Thiol redox transitions in cell signaling, part A: chemistry and biochemistry of low molecular weight and protein thiols*. San Diego, CA: Academic Press (Methods in Enzymology), 117–136. doi: 10.1016/S0076-6879(10)73005-6.

Baler, K., *et al.*, 2014. Electrostatic unfolding and interactions of albumin driven by pH changes: a molecular dynamics study. *The journal of physical chemistry. B*, 118 (4), 921–930. doi: 10.1021/jp409936v.

Batabyal, D., *et al.*, 2021. Determination of the experimental extinction coefficient of therapeutic proteins using the Edelhoch method. *Biologicals*, 71, 42–47. doi: 10.1016/j.biologicals.2021.03.003.

Carter, D.C., *et al.*, 1989. Three-dimensional structure of human serum albumin. *Science*, 244 (4909), 1195–1198. doi: 10.1126/science.2727704.

Chilom, C., *et al.*, 2007. Absorption and fluorescence modifications of tumoral tissue proteins. *Romanian Journal of Biophysics*, 17 (3), 185–193.

Elzoghby, A.O., Samy, W.M., and Elgindy, N.A., 2012. Albumin-based nanoparticles as potential controlled release drug delivery systems. *Journal of controlled release*, 157 (2), 168–182. doi: 10.1016/j.jconrel.2011.07.031.

Farruggia, B. and Picó, G.A., 1999. Thermodynamic features of the chemical and thermal denaturations of human serum albumin. *International journal of biological macromolecules*, 26 (5), 317–323. doi: 10.1016/s0141-8130(99)00054-9.

Ferrari, I.V. and Patrizio, P., 2021. Development and validation molecular docking analysis of human serum albumin (HSA). [Preprint], 1–21. doi: 10.1101/2021.07.09.451789.

Flora, K., *et al.*, 1998. Unfolding of acrylodan-labeled human serum albumin probed by steady-state and time-resolved fluorescence methods. *Biophysical journal*, 75 (2), 1084–1096. doi: 10.1016/S0006-3495(98)77598-8.

Gianazza, E., *et al.*, 1984. The behavior of serum albumin upon isoelectric focusing on immobilized pH gradients. *Electrophoresis*, 5 (5), 310–312. doi: 10.1002/elps.1150050512.

González-Jiménez, J. and Cortijo, M., 2002. Urea-induced denaturation of human serum albumin labeled with acrylodan. *Journal of protein chemistry*, 21 (2), 75–79. doi: 10.1023/A:1014508610017.

Guckeisen, T., Hosseinpour, S., and Peukert, W., 2021. Effect of pH and urea on the proteins secondary structure at the water/air interface and in solution. *Journal of colloid and interface science*, 590, 38–49. doi: 10.1016/j.jcis.2021.01.015.

Hasanbegloo, K., *et al.*, 2023. Paclitaxel-loaded liposome-incorporated chitosan (core)/poly(ε-caprolactone)/chitosan (shell) nanofibers for the treatment of breast cancer. *International journal of biological macromolecules*, 230, 123380. doi: 10.1016/j.ijbiomac.2023.123380.

Hoogenboezem, E.N. and Duvall, C.L., 2018. Harnessing albumin as a carrier for cancer therapies. *Advanced drug delivery reviews*, 130, 73–89. doi: 10.1016/j.addr.2018.07.011.

Hua, L., *et al.*, 2008. Urea denaturation by stronger dispersion interactions with proteins than water implies a 2-stage

unfolding. *Proceedings of the national academy of sciences of the United States of America*, 105 (44), 16928–16933. doi: 10.1073/pnas.0808427105.

Izutsu, K.I., *et al.*, 2009. Stabilization of protein structure in freeze-dried amorphous organic acid buffer salts. *Chemical & pharmaceutical bulletin*, 57 (11), 1231–1236. doi: 10.1248/cpb.57.1231.

Kratz, F., 2008. Albumin as a drug carrier: design of prodrugs, drug conjugates and nanoparticles. *Journal of controlled release*, 132 (3), 171–183. doi: 10.1016/j.jconrel.2008.05.010.

Krissinel, E. and Henrick, K., 2007. Inference of macromolecular assemblies from crystalline state. *Journal of molecular biology*, 372 (3), 774–797. doi: 10.1016/j.jmb.2007.05.022.

Larsen, M.T., *et al.*, 2016. Albumin-based drug delivery: harnessing nature to cure disease. *Molecular and cellular therapies*, 4 (1), 3. doi: 10.1186/s40591-016-0048-8.

Lin, T., *et al.*, 2016. Blood-brain-barrier-penetrating albumin nanoparticles for biomimetic drug delivery via albumin-binding protein pathways for antiglioma therapy. *ACS nano*, 10 (11), 9999–10012. doi: 10.1021/acsnano.6b04268.

Ma, P. and Mumper, R.J., 2013. Paclitaxel nano-delivery systems: a comprehensive review. *J nanomed nanotecghnology*, 4 (2), 1–35. doi: 10.4172/2157-7439.1000164.

Martínez-López, A.L., *et al.*, 2020. Protein-based nanoparticles for drug delivery purposes. *International journal of pharmaceutics*, 581, 119289. doi: 10.1016/j.ijpharm.2020.119289.

Mastropaolo, D., *et al.*, 1995. Crystal and molecular structure of paclitaxel (taxol). *Proceedings of the national academy of sciences of the United States of America*, 92 (15), 6920–6924. doi: 10.1073/pnas.92.15.6920.

McManus, J.J., *et al.*, 2016. The physics of protein self-assembly. *Current opinion in colloid & interface science*, 22, 73–79. doi: 10.1016/j.cocis.2016.02.011.

Möller, M. and Denicola, A., 2002. Protein tryptophan accessibility studied by fluorescence quenching. *Biochemistry and molecular biology education*, 30 (3), 175–178. doi: 10.1002/bmb.2002.494030030035.

Moore, D.S., 1985. Amino acid and peptide net charges: a simple calculational procedure. *Biochemical education*, 13 (1), 10–11. doi: 10.1016/0307-4412(85)90114-1.

Paal, K., Shkarupin, A., and Beckford, L., 2007. Paclitaxel binding to human serum albumin—automated docking studies. *Bioorganic & medicinal chemistry*, 15 (3), 1323–1329. doi: 10.1016/j.bmc.2006.11.012.

Pace, C.N., *et al.*, 1995. How to measure and predict the molar absorption coefficient of a protein. *Protein science*, 4 (11), 2411–2423. doi: 10.1002/pro.5560041120.

Picó, G.A., 1999. Thermodynamic features of the thermal unfolding of human serum albumin. *International journal of biological macromolecules*, 20 (1), 63–73. doi: 10.1016/S0141-8130(96)01153-1.

Protein Data Bank in Europe (2024). Available from: https://www.ebi.ac.uk/pdbe/ [Accessed 30 July 2024].

Ptitsyn, O.B., 1995. Structures of folding intermediates. *Current opinion in structural biology*, 5 (1), 74–78. doi: 10.1016/0959-440x(95)80011-o.

Rabbani, G. and Ahn, S.N., 2019. Structure, enzymatic activities, glycation and therapeutic potential of human serum albumin: a natural cargo. *International journal of biological macromolecules*, 123, 979–990. doi: 10.1016/j.ijbiomac.2018.11.053.

Rabbani, G. and Ahn, S.N., 2021. Review: roles of human serum albumin in prediction, diagnoses and treatment of COVID-19. *International journal of biological macromolecules*, 193 (Pt A), 948–955. doi: 10.1016/j.ijbiomac.2021.10.095.

Rabbani, G., *et al.*, 2017a. Binding of erucic acid with human serum albumin using a spectroscopic and molecular docking study. *International journal of biological macromolecules*, 105 (Pt 3), 1572–1580. doi: 10.1016/j.ijbiomac.2017.04.051.

Rabbani, G., *et al.*, 2017b. Biophysical study on the interaction between eperisone hydrochloride and human serum albumin using spectroscopic, calorimetric, and molecular docking analyses. *Molecular pharmaceutics*, 14 (5), 1656–1665. doi: 10.1021/acs.molpharmaceut.6b01124.

Rabbani, G., *et al.*, 2018. Binding of tolperisone hydrochloride with human serum albumin: effects on the conformation, thermodynamics, and activity of HSA. *Molecular pharmaceutics*, 15 (4), 1445–1456. doi: 10.1021/acs.molpharmaceut.7b00976.

Rowinsky, E.K., 1997. The development and clinical utility of the taxane class of antimicrotubule chemotherapy agents. *Annual review of medicine*, 48, 353–374.

Salem, A.A., *et al.*, 2019. Characterization of human serum albumin's interactions with safranal and crocin using multi-spectroscopic and molecular docking techniques. *Biochemistry and biophysics reports*, 20, 100670. doi: 10.1016/j.bbrep.2019.100670.

Santoro, M.M. and Bolen, D.W., 1988. Unfolding free energy changes determined by the linear extrapolation method. 1. Unfolding of phenylmethanesulfonyl.alpha.-chymotrypsin using different denaturants. *Biochemistry. American chemical society*, 27 (21), 8063–8068. doi: 10.1021/bi00421a014.

Shaw, A.K. and Pal, S.K., 2008. Spectroscopic studies on the effect of temperature on pH-induced folded states of human serum albumin. *Journal of photochemistry and photobiology. B, biology*, 90 (1), 69–77. doi: 10.1016/j.jphotobiol.2007.11.003.

Tayyab, S., Mat, T.N.N.T., and Halim, A.A.A., 2022. Differential stabilizing effects of buffers on structural stability of bovine serum albumin against urea denaturation. *Latin American applied research-an international journal*, 52 (1), 7–13. doi: 10.52292/j.laar.2022.738.

Thao, L.Q., *et al.*, 2017. Doxorubicin and paclitaxel co-bound lactosylated albumin nanoparticles having targetability to hepatocellular carcinoma. *Colloids and surfaces. B, biointerfaces*, 152, 183–191. doi: 10.1016/j.colsurfb.2017.01.017.

Turell, L., *et al.*, 2014. HPLC separation of human serum albumin isoforms based on their isoelectric points. *Journal of chromatography. B, analytical technologies in the biomedical and life sciences*, 944, 144–151. doi: 10.1016/j.jchromb.2013.11.019.

Varma, L.T., *et al.*, 2020. Recent advances in self-assembled nanoparticles for drug delivery. *Current drug delivery*, 17 (4), 279–291. doi: 10.2174/1567201817666200210122340.

Vivian, J.T. and Callis, P.R., 2001. Mechanisms of tryptophan fluorescence shifts in proteins. *Biophysical journal*, 80 (5), 2093–2109. doi: 10.1016/S0006-3495(01)76183-8.

Wang, Z., *et al.*, 2013. Structural studies of several clinically important oncology drugs in complex with human serum albumin. *Biochimica et biophysica acta*, 1830 (12), 5356–5374. doi: 10.1016/j.bbagen.2013.06.032.

Wimalasiri, V.W., *et al.*, 2021. Noyes-Whitney dissolution model-based pH-sensitive slow release of paclitaxel (taxol) from human hair-derived keratin microparticle carriers. *Biomed research international*, 2021 (1), 6657482. doi: 10.1155/2021/6657482.

Zare, E.N. and Makvandi, P., 2019. Self-assembled carbohydrate polymers for food applications: a review. *Comprehensive reviews in food science and food safety*, 18, 2009–2024. doi: 10.1111/1541-4337.12499.